Çukurova Üniversitesi Mühendislik Mimarlık Fakültesi Dergisi, 32(3), ss. 227-241, Eylül 2017
Çukurova University Journal of the Faculty of Engineering and Architecture, 32(3), pp. 227-241, September 2017

Stator Feedforward Voltage Estimation Based Sensorless Permanent Magnet Synchronous Generator Drive using Multi-Parameter Estimation Based on MRAS

Ömer Cihan KIVANÇ[1], Salih Barış ÖZTÜRK[*1]

[1]*Okan Üniversitesi, Mühendislik Fakültesi, Elektrik-Elektronik Mühendisliği Bölümü, İstanbul*

Geliş tarihi: 17.05.2017 Kabul tarihi: 25.09.2017

Abstract

A simple and efficient position sensorless control method based on feedforward voltage estimation for PMSG improved with multi-parameter estimation using MRAS is proposed in this paper. The dynamically enhanced stator feedforward dq–axes voltages that are derived from steady-state PMSG model are modified for the sensorless drive. In direct-drive wind turbine systems, because of low back-EMF amplitude in the generator output at very low speed operation, the rotor flux linkage cannot be predicted correctly. Vector control is often used in PMSG control, because it has a simple structure and is suitable for various industrial systems. In the power equation, maximum power is obtained as a function of torque and speed. In the proposed method, a variable-speed wind turbine system with back to back converter structure is connected to common DC-link. In this paper, the proposed sensorless control scheme has been implemented with 1 kW PMSG drive controlled by a TMS320F28335 DSP for low speed at 0.1 p.u. (300 rpm) is achieved under multi-parameter variations.

Keywords: Model reference adaptive system (MRAS), PMSG, Sensorless control, Feedforward voltage estimation, Multi-parameter estimation

MRAS Tabanlı Çoklu-Parametre Tahmini ile Güçlendirilmiş İleri Beslemeli Stator Gerilim Tahminine Dayanan Sensörsüz Sürekli Mıknatıslı Senkron Generatör Kontrolü

Öz

Bu makalede MRAS tabanlı çoklu-parametre tahmini ile güçlendirilmiş ileri beslemeli stator gerilim tahminine dayanan basit ve verimli bir sensörsüz sürekli mıknatıslı senkron generatör (SMSG) kontrol metodu geliştirilmiştir. Sürekli mıknatıslı senkron generatörün sürekli hal dq–ekseni stator gerilim eşitlikleri önerilen kontrol metoduna uygun olarak ileri beslemeli stator gerilim eşitlikleri haline

[*]Sorumlu yazar (Corresponding author): Salih Barış ÖZTÜRK, *baris.ozturk@okan.edu.tr*

dönüştürülmektedir. Çeşitli endütriyel uygulamalar için uygun ve basit bir yapısı olması nedeniyle SMSG'nin kontrolünde vektör kontrol sıkça kullanılmaktadır. Güç eşitliğinde maksimum güç, moment ve hızın bir fonksiyonu olarak ifade edilir. Önerilen yöntemde, arka arkaya bağlı konvertör yapısına sahip değişken hızlı rüzgar türbini sistemi, ortak DC-baraya bağlanmıştır. Bu makalede, önerilen sensörsüz kontrol metodu TMS320F28335 DSP tarafından kontrol edilen 1 kW PMSG sürücü ile gerçek zamanlı deneysel olarak nominal hızın %10'u (300 rpm) değerindeki düşük hızda çoklu parametre değişimi altında başarı ile gerçekleştirilmiştir.

Anahtar Kelimeler: Model referans adaptif sistem (MRAS), SMSG, Sensörsüz kontrol, İleri beslemeli gerilim tahmini, Çoklu parametre tahmini

1. INTRODUCTION

The difference between fossil energy sources and demanded energy needs is rapidly increasing. This increase leads to alternative search and solutions in energy production. With the integration of smart grid to energy production at the macro level, individual energy production is supported by companies and governments [1]. Utilization of the wind turbines in small energy production is increasing rapidly. In US, the small wind turbine market shares in 2014 reached $60 million. In England, energy capacity of wind turbines ranging between 0 and 1.5 kW is recorded as 1.84 MW in 2013. In small wind turbines, Permanent Magnet Synchronous Generator (PMSG) is preferred for high performance, high power density, reliability, and high efficiency. The outer rotor and the inner rotor PMS generators that have axial flow direction are used in various industries with wide power ranges as direct-drive [2]. In small PMSG systems that generate less than or equal 10 kW power, there is no need for gearbox and the connection can be made directly to the turbine [2–[10]. This is an important factor lowering the cost in small wind turbine systems [8–10]. PMSG is suitable for wind power generation allowing maximum power generation in a wide speed range and at different wind speeds [11]. Efficient wind turbine system can be constructed by adjusting the speed of the generator shaft optimally for variable wind speeds at maximum power operating point [12]. In variable-speed PMSG control, it is required to know the rotor position information and wind speed [13]. Because the working conditions of the turbine changes so often, changes in speed and torque reduce the control performance. Moreover, in order to ensure power generation at wide speed range, sensitive and high resolution position control is performed by encoder, resolver or hall sensors. On the other hand, sensorless PMSG control can be accomplished without using position sensors [10]. In the control of PMSGs, with the elimination of the position sensor, cost, maintenance and robustness problems of the overall system are reduced [8–10]. Because no initial position problem and operating at flux-weakening region exist, sensorless control is a significant cost reductive solution for the control of PMSG drives. Determining the wind speed and rotor position can be accomplished with the methods which are Direct Torque Control (DTC), Model Reference Adaptive System (MRAS), and Sliding Mode Observer (SMO) depending on back-EMF prediction [8, 14–18]. Because these methods are often affected by parameter variation and cause loss of stability at low speeds, they have severe disadvantages in sensorless PMSG control [19–21]. Moreover, because of complex calculation and the difficulty of adjusting control parameters, the methods like EKF, FL and ANN are not preferred in industrial applications [9, 22–27]. Since the amplitude of the back-EMF is poor and fluctuates at low generator operating speeds in sensorless control algorithms that are based on back-EMF estimation, it is difficult to predict the rotor position [28]. Thus, stability of the entire system can be increased and efficient and stable power generation can be achieved at lower speeds. In order to provide parameter adaptation in sensorless control methods, rotor flux linkage estimation and stator resistance adaptation are performed with MRAS, observer based methods, and genetic algorithms [28–32].

In this study, in order to obtain the position and speed information of the driven PMSG directly, feedforward voltage estimation method is suggested. With the proposed method even in the situations where the wind speed is low, it is ensured that a superior PMSG control performance is achieved compared to other sensorless control methods based on back-EMF prediction. Because the rotor flux and the stator resistance undergo a change due to the effects of the loss of magnetic properties of magnets and temperature rise, a highly efficient control is ensured by estimating the rotor flux linkage and stator resistance using MRAS observer [30–34]. In this study, in order to get the maximum efficiency from PMSG, MPPT curve of the wind turbine is obtained in the real system. Active power reference that is required for power control is obtained from this curve after predicting the generator speed. Compared to other position sensorless control algorithms in which the majority of the methods require rotor position estimation first and then the speed is obtained by derivation of the position, in the proposed method primarily the speed is estimated, the position is then estimated with the help of a simple integration and first degree low pass filter without using any derivative term.

This paper is organized as follows. The principle of PMSG and proposed sensorless control method and MPPT studies are presented in Section 2. In Section 3, MRAS method is presented for estimation of stator flux linkage and stator resistance. In Section 4, the proposed speed sensorless control scheme based on MRAS has been implemented with 1 kW PMSG drive controlled by a TMS320F28335 DSP. The hardware implementation and experimental results of the proposed sensorless PM synchronous generator drive including steady-state load disturbance are presented and discussed. Experimental results demonstrate the feasibility and effectiveness of the proposed stator feedforward voltage estimation (FFVE) based position sensorless control scheme improved by MRAS multi-parameter estimation for permanent magnet synchronous generator under various load condition.

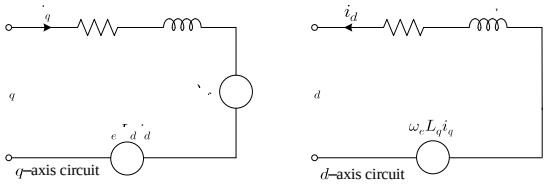

Figure 1. Equivalent electrical circuit diagrams of quadrate q– and d– axes synchronous reference frame of PMSG

2. PROPOSED SENSORLESS CONTROL METHOD AND MPPT STUDIES

The dq model in the rotating synchronous reference frame is used to analyze the PMSG for the proposed speed and position estimations, as shown in Figure 1. The stator voltage equations of the PMSG in the rotating dq reference frame are given by Eq. (1) and Eq. (2), omitting the influences of magnetic field saturation and magnetic hysteresis as

$$v_q=i_qR_s+L_q\frac{di_q}{dt}+(\omega_eL_di_d+\omega_e\lambda_f) \quad (1)$$

$$v_d=i_dR_s+L_d\frac{di_d}{dt}-\omega_eL_qi_q \quad (2)$$

where v_d, v_q, i_d, i_q are the stator d– and q–axes voltages and currents in the rotor reference frame, respectively; R_s is the stator winding resistance; L_d and L_q denote the d– and q–axes inductance, respectively; ω_e is the rotor angular electrical velocity; and λ_f is the flux linkage due to the permanent magnet rotor flux [35, 36]. The steady-state form of dq–axes stator voltage equations can be derived from Eq. (3) and Eq. (4) by making derivative terms equal to zero in each equation as

$$v_q=i_qR_s+(\omega_eL_di_d+\omega_e\lambda_f) \quad (3)$$

$$v_d=i_dR_s-\omega_eL_qi_q \quad (4)$$

2.1. Wind Turbine Characteristics and MPPT Algorithm Based on Indirect Speed Control

The energy produced in wind turbine systems is not only based on the turbine characteristics, but also based on the control method. Output mechanical power of wind turbine is shown as

$$P_{tur}=P_{wind}C_p=\frac{1}{2}\rho\pi r^2 v_w^3 C_p(\lambda,\beta) \quad (5)$$

where ρ is the air density, r is the radius of wind turbine rotor plane, πr^2 is the area swept by the blades, v_w is the wind speed, C_p is the turbine power coefficient, λ is the tip-speed ratio, and β is the pitch angle. In small wind turbines, fixed pitch angle is used because of cost and restrictions. Thus, in Eq. (4), β=0 is assumed. The aerodynamic model of a wind turbine can be characterized by the well-known $C_p(\lambda,\beta)$ curves. λ is defined by

$$\lambda=\frac{\text{Tip Speed}}{\text{Wind Speed}}=\frac{\omega_e r}{v_w} \quad (6)$$

Considering the relationship between λ and C_p as the speed changes for a given wind velocity, there is a unique turbine speed which gives the maximum output power. The peak power for each wind speeds occurs at the point where C_p is maximum. In order to maximize the generated power, it is desirable for the generator to have a power characteristic that follows the maximum C_p curve [18]. C_p is the sixth order polynomial of the tip-speed ratio. C_p curve is modeled based on the sixth order polynomial expression [16]. Curve fitting is a good approximation for wide wind speed values between 2 m/s and 15 m/s. The results of the C_p vs. tip speed ratio λ simulation is shown in Figure 2.

$$C_p(\lambda)=\lambda\left(c_0+\sum_{i=1}^{i=6} c_i\lambda_i\right) \quad (7)$$

$$C_p(\lambda)=c_1\left(\frac{c_2}{\lambda_i}-c_3\beta-c_4\right)e^{\frac{-c_5}{\lambda_i}}+c_6\lambda_i \quad (8)$$

The $C_p(\lambda)$ curves expressed in Eq. (7) and Eq. (8) depend on the blade design and are given by the wind turbine characteristic [13].

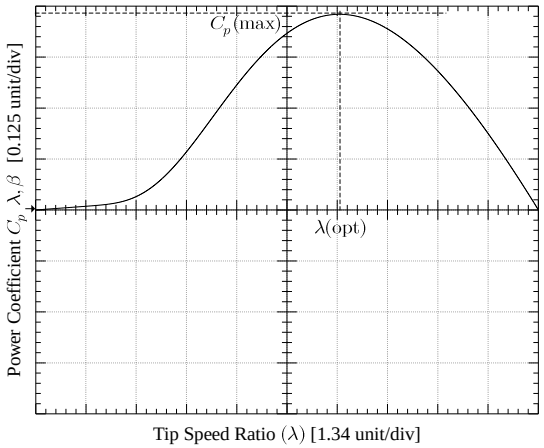

Figure 2. Power coefficient and tip speed ratio curve

The purpose of the proposed sensorless MPPT algorithms is to control the shaft speed of the PMSG to maintain the optimal tip-speed ratio without the knowledge of the PMSG rotor speed and wind speed. In the literature, researchers recommended various methods for sensorless control of PMSG with MPPT control. Optimal torque control, perturbation and observation control, fuzzy logic control and some genetic algorithms are certain methods.

In this study, torque reference is provided by reference speed command called indirect speed control with MPPT [37].

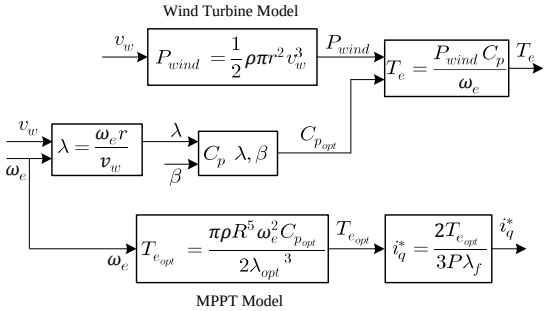

Figure 3. Block diagram of MPPT control algorithm

The prediction of wind speed and rotor speed are important parameters for maximum power output. To obtain maximum active power for variable wind speed, λ_{opt} can be calculated from the roots of the derivative of the polynomial in Eq. (8). Then, based on the reference wind speed v_w the corresponding optimal generator speed is obtained. Figure 2 shows that the proposed MPPT algorithm is based on the reference wind turbine. The equation Eq. (9) shows torque calculation based on P_{wind} and C_p.

$$T_e=\frac{3p}{2}\lambda_f i_q=\frac{P_{wind}C_p}{\omega_e} \tag{9}$$

Reference current is generated from the outer voltage loop via regulating the DC-link voltage based on control error. In both voltage control loops, the PI feedback controllers are enhanced simply by robust control scheme, as shown in Figure 3 to yield good dynamic performance. Reference current is generated based on the specific wind speed with MPPT mechanism. In order to produce maximum DC-power in DC-link at variable speeds, proposed sensorless control method that is capable of obtaining precise position estimation at different wind speeds is proposed.

$$T_{e_{opt}}=\frac{\pi\rho R^5\omega_e{}^2C_{p_{opt}}}{2\lambda_{opt}{}^3} \tag{10}$$

$$i_q{}^*=\frac{2T_{e_{opt}}}{3p\lambda_f}=\frac{\pi C_{p_{opt}}R^5\omega_e{}^2}{3p\lambda_f\lambda_{opt}{}^3} \tag{11}$$

The equations Eq. (10) and Eq. (11) show optimal torque and optimal q–axis current command that are given as reference variable wind speed.

dq–axes stator feedforward voltages are normally used in the FOC of AC machines at the output of the inner dq–axes PI current regulators to enhanced the dynamic performance of the machine [38]. In this method, feedforward voltages are not only used for the dynamic performance improvements, but also used to achieve a simple but effective position sensorless speed control of PMSG drive.

It is visible that stator d– and q–axes currents can be controlled by the d– and q–axes voltages and speed ω using Eq. (12) and Eq. (13). The control principle is adopted where the current in q–axis is controlled by speed of rotation or frequency of stator voltage applied to q–axis winding [19]. The amplitude of q–axis voltage is obtained by neglecting the derivative term and assuming that real currents closely follow reference values $i_q=i_q^*$ and $i_d=i_d^*$ (reference values are marked with * in the superscript and hat ^ above is the symbol indicates estimates) [38]. Below are the modified stator feedforward voltage equations for the proposed speed sensorless scheme given in dq reference frame,

$$v_q^*=i_q^*\hat{R}_s+\left(\omega_e L_d i_d^*+\omega_e\hat{\lambda}_f\right)+K\Delta v \tag{12}$$

$$v_d^*=i_d^*\hat{R}_s-\omega_e L_q i_q^*+\Delta v \tag{13}$$

where Δv is the output of the d–axis PI current regulator and ω_e is the output of the q–axis PI current regulator. Δv is multiplied by gain K and added to q–axis voltage equation v_q^* representing the part of the derivative term in the dynamic voltage equation given in (1). Similarly, Δv term in Eq. (12) also acts as the derivative representation given in Eq. (2) for achieving a better transient response in the sensorless operation.

The dq frame stator voltages given in Eq. (12) and Eq. (13) are obtained by modifying the dynamic machine model and used as the basic reference signals to control the PM machine without requiring a position sensor. The signals depend on machine parameters. At any operating point, the machine itself determines the required voltages at its terminal by letting the inverter duplicate the voltages. This process is so called as self-control. The components of the dq frame voltage reference signals given in Eq. (12) and Eq. (13) are derived from Eq. (1) and Eq. (2), respectively under the assumption of steady-state conditions where

derivative terms are replaced with the regulator correction terms and a relevant gain.

In stator voltage estimation, stator resistance is arranged depending on the error between reference d–axis current and feedback d–axis current component. Since the stator resistance variation has a minimal effect on the control, the method provides high dynamic control capability. Moreover, q–axis current is controlled by speed feedback. The method proposed by Okuyama et al. [39] has been applied for induction machine. The variation of the rotor flux linkage is estimated by observer and updated online. According to the proposed method based on stator voltage estimation, the voltage signal is added to v_q as a feedforward signal. In this study, a high performance sensorless operation is performed in a wide speed range without using high-frequency signal injection. In speed estimation, Δv is taken as the reference which varies proportional to speed. In the proposed method, while the stator resistance change effects are not taken into consideration continuously, the rotor flux linkage variation determines the performance of the proposed control method [33, 40]. The rotor flux linkage is controlled by an additional feedforward voltage signal. K value is a gain which is determined based on the variable speed region. Start-up performance of the generator relies on K value that should be fixed properly as an important parameter in the proposed sensorless control.
Note that estimation of rotor speed $\hat{\omega}_r$ is obtained by passing ω_e obtained from output of the PI current regulator in q–axis through a first order filter. The time constant of the filter depends on the overall system mechanical characteristics and heavily affects the dynamics and stability of the sensorless control scheme.

3. ROTOR FLUX LINKAGE AND STATOR RESISTANCE ESTIMATOR BASED ON MRAS

PMSG motor parameters vary depending on temperature, frequency, load conditions and work zone [41, 42]. In order to eliminate the effects of parameter changes, an MRAS observer structure is suggested for the proposed sensorless control scheme. While the rotor position errors occur from stator resistance change at low speeds, this problem is eliminated with multi-parameter estimation; the effects of the rotor flux linkage change caused from permanent magnets are also eliminated [43–45].

A high performance PI regulator is used for PMSM sensorless speed control; for low speeds and transients an adaptive MRAS observer is used, as shown in Figure 4. In addition to rotor flux linkage and stator resistance change, feedforward voltage estimation method is used together with MRAS in order to eliminate disturbance effects in position estimation. Principally, MRAS depends on the principle that reference and estimation models are compared and the obtained error is regulated by an adaptive model until stability is achieved [46].

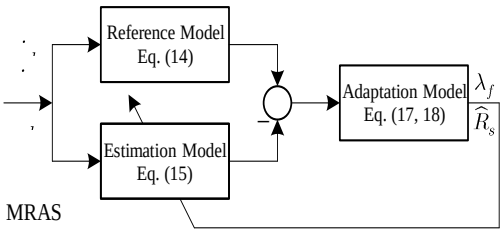

Figure 4. MRAS principle block diagram

MRAS adaptation mechanism estimates slowly varying parameters based on the hyperstability theory [47]. In the proposed method, MRAS is superior to feedforward voltage estimation. It provides prevention of disruptive effects caused from parameter variation. MRAS basic equation consists of feedforward linear model and non–linear feedback components. G_1 and G_2 coefficient in G matrix ensures feedforward linear model to be a positive and real number [48]. Non-linear block is solved according to POPOV integral equation. Equations for reference and estimation models shown in Figure 4 are expressed in Eq. (14) and Eq. (15), respectively.

$$\begin{bmatrix}\frac{di_q}{dt}\\ \frac{di_d}{dt}\end{bmatrix}=\underbrace{\begin{bmatrix}\frac{-R_s}{L_q} & \frac{-L_d}{L_q}\omega_e\\ \frac{L_q}{L_d}\omega_e & \frac{-R_s}{L_d}\end{bmatrix}}_{A}\begin{bmatrix}i_q\\ i_d\end{bmatrix}+\underbrace{\begin{bmatrix}\frac{1}{L_q} & 0\\ 0 & \frac{1}{L_d}\end{bmatrix}}_{B}\begin{bmatrix}v_q\\ v_d\end{bmatrix}+\underbrace{\begin{bmatrix}\frac{-\lambda_f}{L_q}\omega_e\\ 0\end{bmatrix}}_{C} \quad (14)$$

$$\begin{bmatrix}\frac{d\hat{i}_q}{dt}\\ \frac{d\hat{i}_d}{dt}\end{bmatrix}=\underbrace{\begin{bmatrix}\frac{-\hat{R}_s}{L_q} & \frac{-L_d}{L_q}\omega_e\\ \frac{L_q}{L_d}\omega_e & \frac{-\hat{R}_s}{L_d}\end{bmatrix}}_{\hat{A}}\begin{bmatrix}\hat{i}_q\\ \hat{i}_d\end{bmatrix}+\underbrace{\begin{bmatrix}\frac{1}{L_q} & 0\\ 0 & \frac{1}{L_d}\end{bmatrix}}_{\hat{B}}\begin{bmatrix}v_q\\ v_d\end{bmatrix}+\underbrace{\begin{bmatrix}\frac{-\hat{\lambda}_f}{L_q}\omega_e\\ 0\end{bmatrix}}_{\hat{C}}+\underbrace{\begin{bmatrix}G_1 & 0\\ 0 & G_2\end{bmatrix}}_{G}\begin{bmatrix}\hat{i}_q-i_q\\ \hat{i}_d-i_d\end{bmatrix} \quad (15)$$

where $\hat{R}_s$ and $\hat{\lambda}_f$ are the estimated stator resistance and rotor flux linkage, respectively which are the outputs of the adaptation model. $\hat{R}_s$ and $\hat{\lambda}_f$ are updated in the estimation block in the closed loop system, as a result $\hat{i}_q$ and $\hat{i}_d$ currents are predicted.

$$\dot{e}=\begin{bmatrix}\frac{d(\hat{i}_q-i_q)}{dt}\\ \frac{d(\hat{i}_d-i_d)}{dt}\end{bmatrix}=\left(\begin{bmatrix}\frac{-R_s}{L_q} & \frac{-L_d}{L_q}\omega_e\\ \frac{L_q}{L_d}\omega_e & \frac{-R_s}{L_d}\end{bmatrix}+\begin{bmatrix}G_1 & 0\\ 0 & G_2\end{bmatrix}\right)\begin{bmatrix}\hat{i}_q-i_q\\ \hat{i}_d-i_d\end{bmatrix}+\left(\begin{bmatrix}\frac{-R_s}{L_q} & \frac{-L_d}{L_q}\omega_e\\ \frac{L_q}{L_d}\omega_e & \frac{-R_s}{L_d}\end{bmatrix}-\begin{bmatrix}\frac{-\hat{R}_s}{L_q} & \frac{-L_d}{L_q}\omega_e\\ \frac{L_q}{L_d}\omega_e & \frac{-\hat{R}_s}{L_d}\end{bmatrix}\right)\begin{bmatrix}\hat{i}_q\\ \hat{i}_d\end{bmatrix}+\left(\begin{bmatrix}\frac{-\lambda_f}{L_q}\omega_e\\ 0\end{bmatrix}-\begin{bmatrix}\frac{-\hat{\lambda}_f}{L_q}\omega_e\\ 0\end{bmatrix}\right) \quad (16)$$

In Eq. (16), the errors of the MRAS current estimators are given. Selection of accurate values of G_1 and G_2 gains given in Eq. (15) eliminate the algebraic loop problem occurs in simulation and experimental studies [48]. The error correction is accomplished by an adaptation model. G matrix given in Eq. (15) is an observer gain matrix in which the parameters should be adjusted properly [46]. False selection of the G matrix parameters causes algebraic loops. Adaptation equations for $\hat{R}_s$ and $\hat{\lambda}_f$ are given in Eq. (17) and Eq. (18), respectively where $k_{p_{res}}$, $k_{i_{res}}$, $k_{p_{flux}}$, $k_{i_{flux}}$, $\hat{R}_0$, $\hat{\lambda}_{f0}$ are the estimated resistance proportional regulator coefficient, estimated resistance integrator regulator coefficient, estimated rotor flux linkage proportional regulator coefficient, rotor flux linkage integrator regulator coefficient, and the estimated previous stator resistance and rotor flux linkage, respectively.

$$\hat{R}_s=-\left(k_{p_{res}}+\frac{k_{i_{res}}}{s}\right)\left(L_s\hat{i}_d\left(i_d-\hat{i}_d\right)+\hat{i}_q\left(i_q-\hat{i}_q\right)\right)+\hat{R}_0 \quad (17)$$

$$\hat{\lambda}_f=-\left(k_{p_{flux}}+\frac{k_{i_{flux}}}{s}\right)\omega_e\left(i_q-\hat{i}_q\right)L_s+\hat{\lambda}_{f0}. \quad (18)$$

Stator resistance and rotor flux linkage estimation values in Eq. (17) and Eq. (18) guarantees to give faster response than the closed loop cycle. Since large selected state errors are constantly growing and small selected estimation time gets longer, selection of proper regulator parameters are crucial for minimizing the steady-state error [49]. In the proposed MRAS method, a low-pass filter (LPF) is used to overcome the rise of the estimated rotor flux linkage value at low speed and at zero crossing and distortion effects caused from stator resistance estimation. In the situations where LPF is not used at low speed, the estimation values are small and cause the output of the feedforward voltage estimation values to be faulty [50].

4. EXPERIMENTAL RESULTS

To show validity of the proposed control scheme, the experimental studies are carried out for the systems shown in Figure 5 under various operation

conditions. A sensorless drive system for a PMSG, in which stator resistance and rotor flux linkage variation are estimated, is proposed in this section. In this study, the value of stator resistance and rotor flux linkage are estimated using MRAS. However, inductance variation is neglected because the influence of the q–axis inductance is independent from the speed and position estimation, but variation of stator resistance and rotor flux linkage increases errors in low speed region. Figure 6 shows the schematic diagram of the proposed overall control system. The complete system is experimented for various conditions. The control algorithm is implemented on TMS320F28335 DSP and the proposed method is validated through experimental results.

In PMSG sensorless drive system, stator resistance and flux linkage variation depend on temperature rise and affect the sensorless control. These parameters are estimated using MRAS in order to improve the accuracy of position estimation.

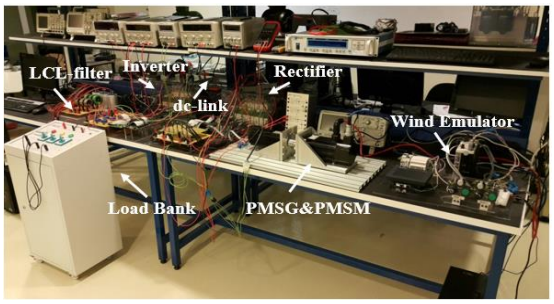

Figure 5. Experimental test-bed

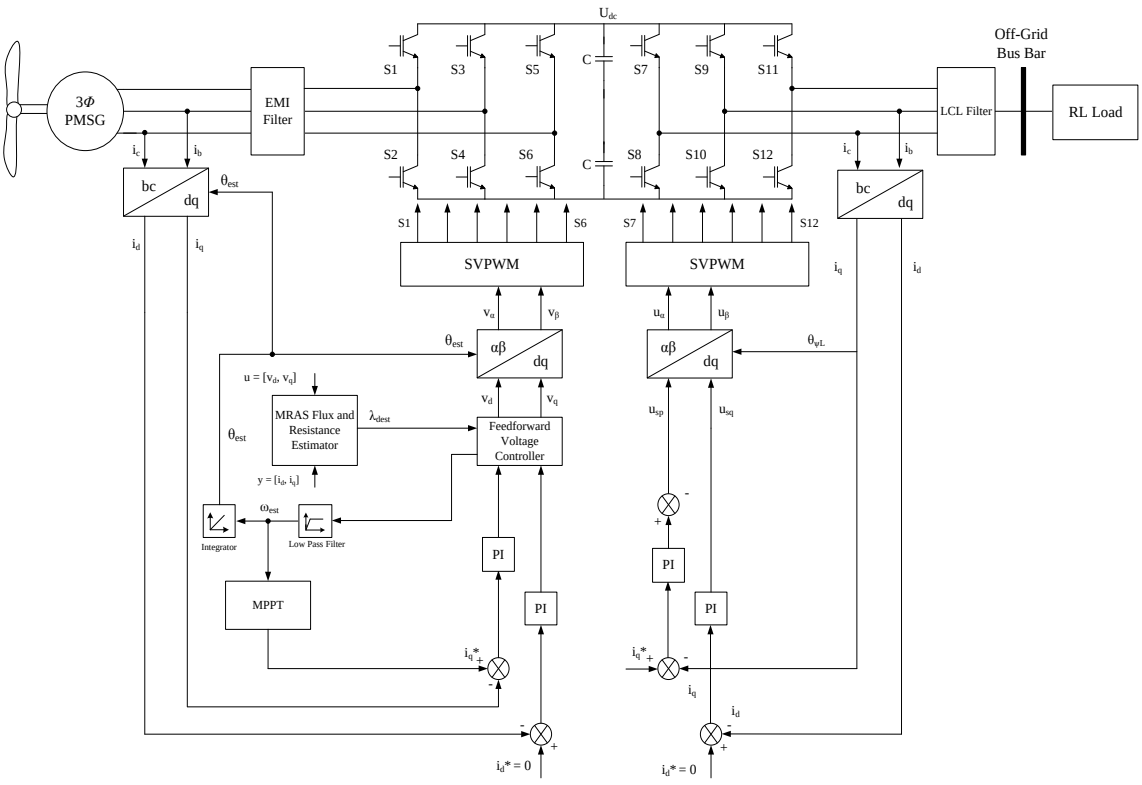

Figure 6. Overall block diagram of proposed sensorless PMSG drive model based on MRAS parameter estimation

The parameter estimation of the stator resistance and rotor flux linkage is important because of their effects in the reference PMSM equations shown in Eq. (1) and Eq. (2). The experimental results verify the validity of the parameter estimation and the effectiveness of the proposed sensorless control

system. Figure 7 and Figure 8 show variations in the estimated stator resistance measured initially as 3.4 Ω and rotor flux linkage as 0.094 Wb during the experiment, respectively.

While the stator resistance is measured as about 3.4 Ω, it has been observed that it reaches to 3.77 Ω depending on thermal change during the experiment. This corresponds to the pre-estimated temperature values. In case of demands of high current in wind turbines, stator resistance changes depend on the temperature. Therefore, the stator winding temperature estimation can be modeled as

$$T_{est}=\frac{\hat{R}_s-R_0}{R_0\alpha}+T_0 \quad (19)$$

where, R_0 is the initial resistance value at temperature T_0, $\hat{R}_s$ is the estimated stator winding resistance at temperature T_{est} using MRAS and α is the temperature coefficient of copper ($3.93x10^{-3}$ per °C). Point temperature measurements has revealed to be 44 °C on the surface temperature. When the estimated stator resistance value is placed in Eq. (19), it is seen that the estimated temperature has been calculated to be 47 °C. Considering that the temperature of stator winding is high, estimated stator resistance value is proved to be correct. The estimation error of the position and speed appears at the transient state. However, at steady-state speed and position, errors decrease and stable sensorless PMSG control is achieved.

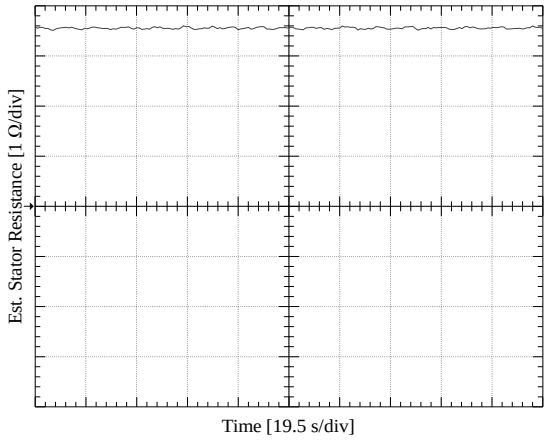

Figure 7. Estimated initial stator resistance

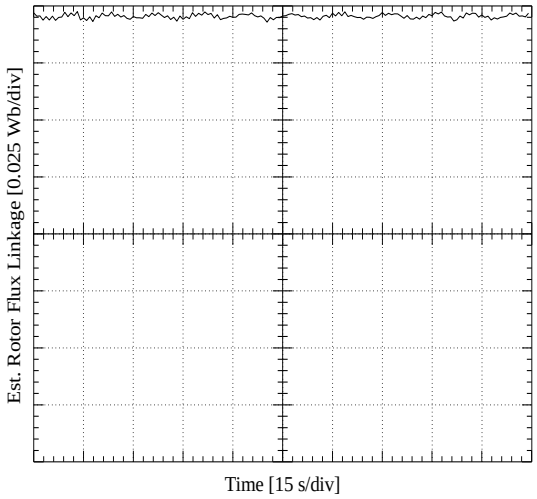

Figure 8. Estimated initial rotor flux linkage

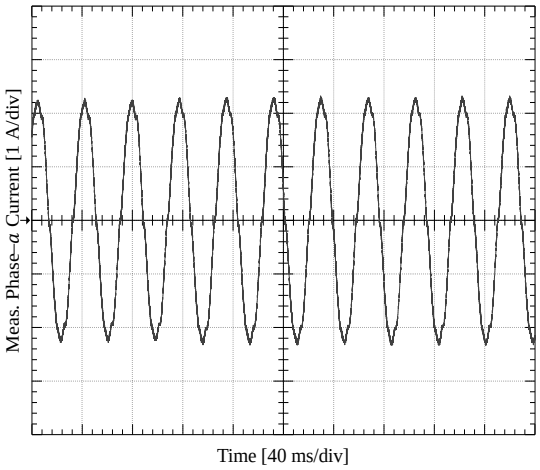

Figure 9. Experimental PMSG phase–*a* current, (U_{DC} = 50 V) and (R_{Load} = 22 Ω)

In Figure 9, phase–*a* current waveform of PMSG driven at 400 r/min under 50 V DC-link is represented. U_{DC} is the DC-link voltage of PMSG forming at the power stage output. Measurements have been done by connected loads (R_{Load} = 22 Ω) to the DC-link that PMSG is connected to, and current with 2.28 A peak value has been obtained. Figure 10 shows phase–*a* current for PMSG driven at 1050 r/min. Measurements have been done by connecting the load (R_{Load} = 43 Ω) to the DC-link and current with 2.12 A peak value has been obtained.

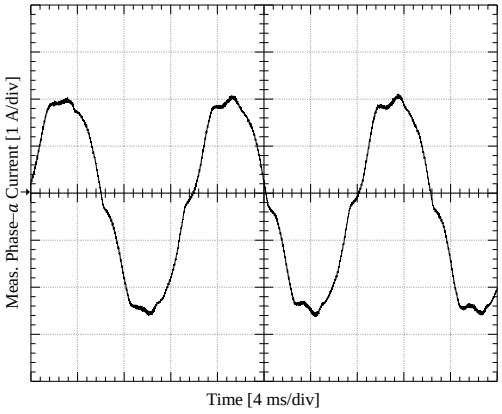

Figure 10. Experimental PMSG phase–*a* current (U_{DC} = 100 V) and (R_{Load} = 43 Ω)

In Figure 11, off-grid generator measurements are seen. "m" represents modulation index which is defined by the rate of the reference signals and the carrier signal amplitudes. The peak phase–*a* to phase–*c* voltage has been measured as 117 V. Phase–*a* current has been measured to be 2.8 A. DC-link voltage can be controlled by calculating the peak voltage value at the DC-link using Eq. (20).

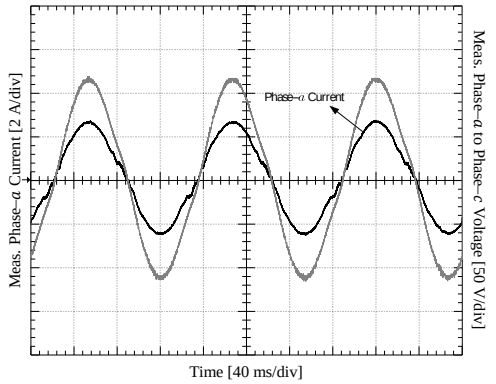

Figure 11. Experimental off-grid side phase–*a* current and phase–*a* to phase–*c* voltage for m = 0.6, (U_{DC} = 225 V) and (R_{Load} = 43 Ω)

The RMS value of 117 V phase voltage ($V_{LL(rms)}$) is 82.73 V, and the DC-link voltage (m = 0.6) is 225 V. In Figure 11, R_{Load} = 43 Ω which is connected as star has been used at the *LCL* filter output.

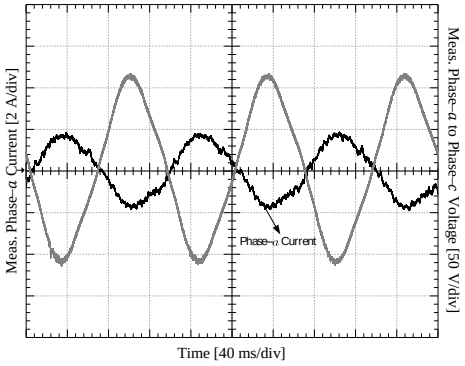

Figure 12. Experimental off-grid side phase–*a* current and phase–*a* to phase–*c* voltage for m = 0.6, (U_{DC} = 225 V) and (R_{Load} = 43 Ω and L_{Load} = 50 mH)

$$U_{DC} = 2\sqrt{2}V_{LL(rms)}/(\sqrt{3}m) \quad (20)$$

In Figure 12, phase–*a* current for the off-grid part of PMSG driven at 1000 r/min, and the voltage waveform of phase–*a* to phase–*b* are illustrated. While phase to phase peak voltage value is 117 V, the DC-link voltage has been measured as 225 V. Resistive and inductive loads have been connected to the *LCL* filter output.

In Figure 13, phase–*a* current for the off-grid side of PMSG driven at 500 r/min, and the voltage waveform of phase–*a* to phase–*b* are shown. Phase to phase peak voltage value is 73 V and the DC-link voltage has been measured as 210 V.

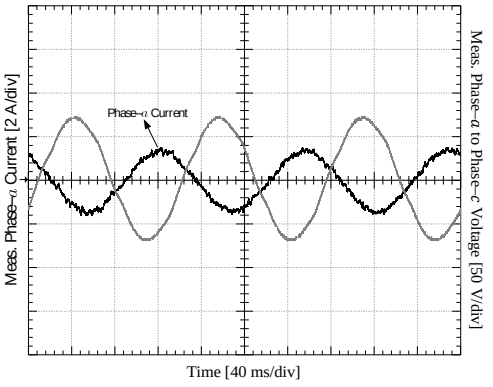

Figure 13. Experimental off-grid side phase–*a* current and phase–*a* to phase–*b* voltage for m = 0.4, (U_{DC} = 210 V) and (R_{Load} = 43 Ω and L_{Load} = 50 mH)

In Figure 14, phase–*c* current and voltage modulation index of phase–*a* to phase–*c* has been adjusted to be 1.0 for the same conditions. Under this working condition, phase to phase peak value of voltage is 101 V, and the peak current value is 2.1 A.

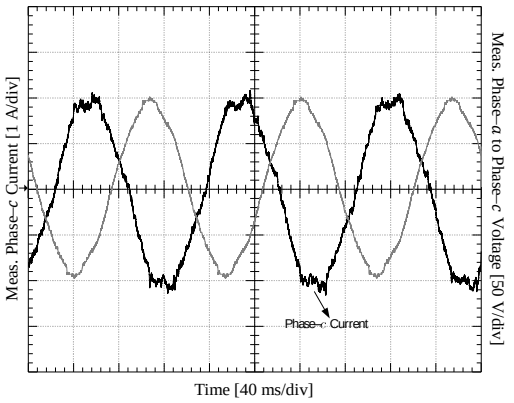

Figure 14. Experimental off-grid side phase–*c* current and phase–*a* to phase–*c* voltage for m = 1.0, (U_{DC} = 210 V) and (R_{Load} = 43 Ω and L_{Load} = 50 mH)

In Figure 15, phase–*c* current for the off-grid side of PMSG driven at 300 r/min and voltage waveform of phase–*a* to phase–*c* are given. Peak phase to phase voltage value has been measured as 51 V while DC-link voltage is 59 V and phase–*c* current is 1.28 A.

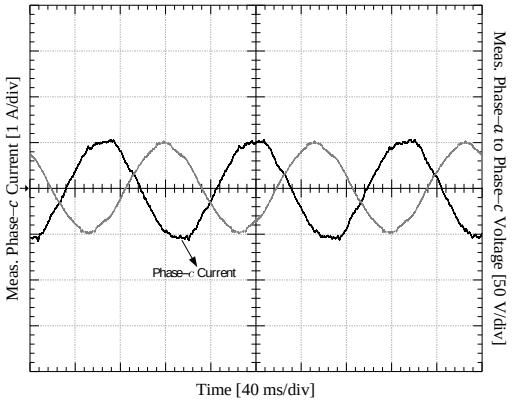

Figure 15. Experimental off-grid side phase–*c* current and phase–*a* to phase–*c* voltage for m = 1.0, (U_{DC} = 59 V) and (R_{Load} = 43 Ω and L_{Load} = 50 mH)

In Figure 16, phase–*c* current for the off-grid side of PMSG driven at 400 r/min and voltage waveform of phase–*a* to phase–*c* are illustrated. Peak phase to phase voltage value has been measured as 79 V while DC-link voltage is 91 V and phase–*c* current is 1.88 A.

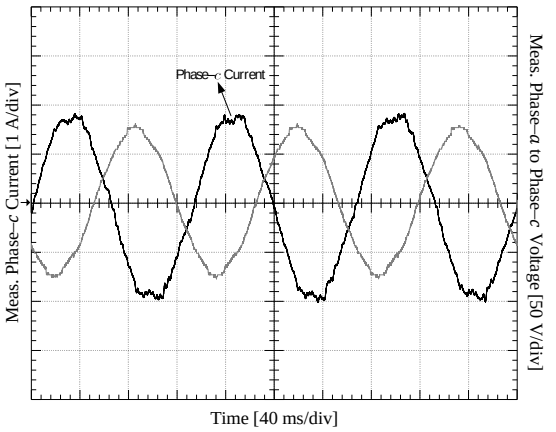

Figure 16. Experimental off-grid side phase–*c* current and phase–*a* to phase–*c* voltage for m = 1.0, (U_{DC} = 59 V) and (R_{Load} = 43 Ω and L_{Load} = 50 mH)

In Figure 17, phase–*c* current of the off-grid side of PMSG driven at 750 r/min and voltage waveform of phase–*a* to phase–*c* are given.

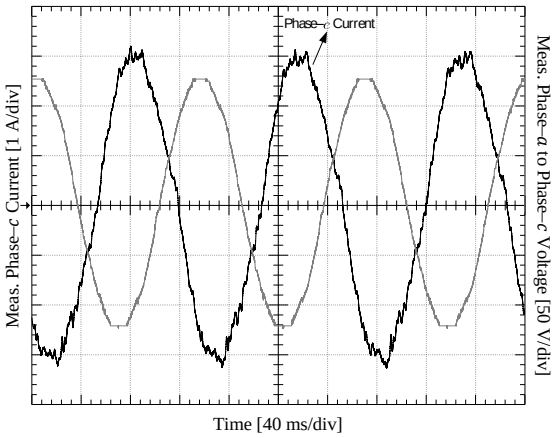

Figure 17. Experimental off-grid side phase–*c* current and phase–*a* to phase–*c* voltage for m = 1.0, (U_{DC}= 127 V) and (R_{Load}= 43 Ω and L_{Load}=50 mH)

Peak voltage value between phase–*a* to phase–*c* has been measured as 127 V while DC-link voltage is 147 V and phase–*c* current is 3.24 A. Measurements reflect that THD of the voltage between phase–*a* to phase–*b* at the *LCL*-filter input in the off-grid side of SSTP (assuming there is no *LCL* filter) is 51.15% and it is considered too high. The THD of the voltage phase–*a* to phase–*b* at the *LCL* filter output in the off-grid side of SSTP is around 4%.

4. CONCLUSION

The rotor flux linkage that changes due to aging, vibration, humidity and temperature reduces the drive control performance. So, the effects of aging are tried to be eliminated and the control performance is increased with life estimation algorithms in the literature using online-learning methods and parameter estimation methods. Because the rotor flux and the stator resistance undergo a change due to the effects of the loss of magnetic properties of magnets and temperature rise, a highly efficient control is ensured by estimating the rotor flux linkage and stator resistance using MRAS observer. In order to obtain the position and speed information of the driven PMSG directly, feedforward voltage estimation method is suggested. With the proposed method even in the situations where the wind speed is low, it is ensured that a superior PMSG control performance compared to other sensorless control methods based on back-EMF prediction is achieved.

Using the proposed method, maximum power generation with 4% THD in the line voltages is achieved by using the designed LCL filter compared to other back-EMF estimation methods even under low wind speeds at 0.1 p.u. (300 rpm) of the PMSG drive.

5. ACKNOWLEDGMENTS

This work was supported by The Scientific and Technological Research Council of Turkey (TUBITAK) funded project (112E263).

APPENDIX

Parameters of the PM Synchronous Machine

Number of poles	: 8
Rated torque (N·m)	: 2
Rated rms current (A)	: 4
Stator inductance (mH)	: 0.0033
Stator resistance (Ω)	: 3.4
Rotor magnetic flux linkage (Wb)	: 0.095
Moment of inertia (kg.m^2)	: 0.0075

6. REFERENCES

1. Dasgupta, S., Mohan, S.N., Sahoo, S.K. Panda, S.K., 2013. Application of Four-Switch-Based Three-Phase Grid-Connected Inverter to Connect Renewable Energy Source to a Generalized Unbalanced Microgrid System. IEEE Transactions on Industrial Electronics, 60(3), 1204–1215.

2. Iov, F., Blaabjerg, F., 2009. Power Electronics and Control for Wind Power Systems, IEEE Power Electronics and Machines in Wind Applications, PEMWA, 1–16.

3. Parviainen, A., Pyrhonen, J., Kontkanen, P., 2005. Axial Flux Permanent Magnet Generator with Concentrated Winding for Small Wind Power Applications, 1187–1191.

4. Bumby, J.R., Stannard, N., Dominy, J., McLeod, N., 2008. A Permanent Magnet Generator for Small Scale Wind and Water Turbines, 1–6.

5. Andriollo, M., De Bortoli, M., Martinelli, G., Morini, A., Tortella, A., 2008. Permanent Magnet Axial Flux Disc Generator for Small Wind Turbines, 1–6.

6. Olano, A., Moreno, V., Molina, J., Zubia, I., 2008. Design and Construction of an Outer-Rotor PM Synchronous Generator for Small Wind Turbines; Comparing Real Results with Those of FE Model, 1–6.

7. Haraguchi, H., Morimoto, S., Sanada, M., 2009. Suitable Design of a PMSG for a Small-Scale Wind Power Generator, 1–6.

8. Zhang, Z., Zhao, Y., Qiao, W., Qu, L., 2014. A Space-Vector-Modulated Sensorless Direct-Torque Control for Direct-Drive PMSG Wind

Turbines, IEEE Transactions on Industry Applications, 50(4), 2331–2341.

9. Benadja, M., Chandra, A., 2014. Sensorless Control for Wind Energy Conversion System (WECS) with Power Quality Improvement, IEEE PES General Meeting| Conference & Exposition, 1–5.

10. Hu, K.W., Liaw, C.M., 2015. Position Sensorless Surface-Mounted Permanent-Magnet Synchronous Generator and its Application to Power DC Microgrid. IET Power Electronics, 8(9), 1636–1650.

11. Baroudi, J.A., Dinavahi, V., Knight, A.M., 2007. A Review of Power Converter Topologies for Wind Generators. Renewable Energy, 32(14), 2369–2385.

12. Muller, S., Deicke, M., De Doncker, R.W., 2002. Doubly Fed Induction Generator Systems for Wind Turbines. IEEE Industry Applications Magazine, 8(3), 26–33.

13. Qiao, W., Zhou, W., Aller, J.M., Harley, R.G., 2008. Wind Speed Estimation Based Sensorless Output Maximization Control for A Wind Turbine Driving a DFIG. IEEE Transactions on Power Electronics, 23(3), 1156–1169.

14. Guo, L., Zhang, X., Yang, S., Xie, Z., Qi, L., Wang, L., 2015. Super-Twisting Sliding Mode Observer Based Speed Sensorless Torque Control for PMSG Used in Wind Turbines, 2457–2462.

15. Ding, Z., Wei, G., Ding, X., 2014. PMSM Control System Based on Sliding Mode Technology and MRAS Method. IEEE International Conference on Mechatronics and Control (ICMC), 1276–1281.

16. Koch, G., Gabbi, T., Henz, G., Vieira, R.P., Pinheiro, H., 2015. Sensorless Technique Applied to PMSG Of WECS Using Sliding Mode Observer. IEEE 13th Brazilian Power Electronics Conference and 1st Southern Power Electronics Conference (COBEP/SPEC), 1–6.

17. Han, Y.S., Choi, J.S., Kim, Y.S., 2000. Sensorless PMSM Drive with a Sliding Mode Control Based Adaptive Speed and Stator Resistance Estimator. IEEE Transactions on Magnetics, 36(5), 3588–3591.

18. Yan, J., Lin, H., Feng, Y., Guo, X., Huang, Y., Zhu, Z.Q., 2013. Improved Sliding Mode Model Reference Adaptive System Speed Observer for Fuzzy Control of Direct-Drive Permanent Magnet Synchronous Generator Wind Power Generation System. IET Renewable Power Generation, 7(1), 28–35.

19. Akatsu, K., Kawamura, A., 2000. Sensorless Very Low-Speed and Zero-Speed Estimations with Online Rotor Resistance Estimation of Induction Motor Without Signal Injection. IEEE Transactions on Industry Applications, 36(3), 764–771.

20. Eskola, M., Tuusa, H., 2003. Comparison of MRAS and Novel Simple Method for Position Estimation in PMSM Drives, vol. 2, 550–555.

21. Burth, M., Verghese, G.C., Vélez-Reyes, M., 1999. Subset Selection for Improved Parameter Estimation in On-line Identification of a Synchronous Generator, IEEE Transactions on Power Systems, 14(1), 218–225.

22. Liu, K., Zhu, Z.Q., Stone, D.A., 2013. Parameter Estimation for Condition Monitoring of PMSM Stator Winding and Rotor Permanent Magnets, IEEE Transactions on Industrial Electronics, 60(12), 5902–5913.

23. Chan, T.F., Wang, W., Borsje, P., Wong, Y.K., Ho, S.L., 2008. Sensorless Permanent-Magnet Synchronous Motor Drive Using a Reduced-Order Rotor Flux Observer. IET Electric Power Applications, 2(2), 88–98.

24. Rigatos, G., Siano, P., Zervos, N., 2014. Sensorless Control of Distributed Power Generators with the Derivative-free Nonlinear Kalman Filter, IEEE Transactions on Industrial Electronics, 61(11), 6369–6382.

25. Shasadeghi, M., Mardanah, M., Nayeripour, M., Mansuri, M., 2015. Sensor Less Control of PMSG-based Wind Turbine with Parallel Distributed Compensator with Fuzzy Observer, 35–40.

26. Benadja, M., Chandra, A., 2015. Adaptive Sensorless Control of Pmsgs-Based Offshore Wind Farm and VSC-HVDC Stations, IEEE Journal of Emerging and Selected Topics in Power Electronics, 3(4), 918–931.

27. Li, H., Shi, K.L., McLaren, P.G., 2005. Neural-Network-Based Sensorless Maximum Wind Energy Capture with Compensated Power Coefficient. IEEE Transactions on Industry Applications, 41(6), 1548–1556.

28. Inoue, Y., Yamada, K., Morimoto, S., Sanada, M., 2007. Accuracy Improvement of IPMSM Sensorless Drives with On-line Parameter Identification, 860–866.

29. Colovic, I., Kutija, M., Sumina, D., 2014. Rotor Flux Estimation for Speed Sensorless Induction Generator Used in Wind Power Application, 23–27.

30. Liu, K., Zhu, Z.Q., 2014. Online Estimation of the Rotor Flux Linkage and Voltage-source Inverter Nonlinearity in Permanent Magnet Synchronous Machine Drives, IEEE Transactions on Power Electronics, 29(1), 418–427.

31. Lei, T., Barnes, M., Smith, S., Hur, S.H., Stock, A., Leithead, W.E., 2015. Using Improved Power Electronics Modeling and Turbine Control to Improve Wind Turbine Reliability. IEEE Transactions on Energy Conversion, 30(3), 1043–1051.

32. Jung, S.M., Park, J.S., Kim, H.W., Cho, K.Y., Youn, M.J., 2013. An MRAS-Based Diagnosis of Open-circuit Fault in PWM Voltage-source Inverters for PM Synchronous Motor Drive Systems, IEEE Transactions on Power Electronics, 28(5), 2514–2526.

33. Xiao, X., Chen, C., Zhang, M., 2010. Dynamic Permanent Magnet Flux Estimation of Permanent Magnet Synchronous Machines. IEEE Transactions on Applied Superconductivity, 20(3), 1085–1088.

34. Dumnic, B., Katic, V., Vasic, V., Milicevic, D., Delimar, M., 2012. An Improved MRAS Based Sensorless Vector Control Method for Wind Power Generator, Journal of Applied Research and Technology, 10(5), 687–697.

35. Bose, B.K., 1997. Power Electronics and Variable Frequency Drives: Technology and Applications, 36–76.

36. Krishnan, R., 2009. Permanent Magnet Synchronous and Brushless DC Motor Drives, CRC Press.

37. Diaz, S.A., Silva, C., Juliet, J., Miranda, H.A., 2009. Indirect Sensorless Speed Control of a PMSG for Wind Application, 1844–1850.

38. Holtz, J., 2002. Sensorless Control of Induction Motor Drives, Proceedings of the IEEE, 90(8), 1359–1394.

39. Okuyama, T., Fujimoto, N., Fujii, H., 1990. A Simplified Vector Control System Without Speed and Voltage Sensors-effect of Setting Errors of Control Parameters and Their Compensation. Electrical Engineering in Japan, 110(4), 129–139.

40. Akatsu, K., Kawamura, A., 2000. Online Rotor Resistance Estimation Using the Transient State Under the Speed Sensorless Control of Induction Motor, IEEE Transactions on Power Electronics, 15(3), 553–560.

41. Underwood, S.J., Husain, I., 2010. Online Parameter Estimation and Adaptive Control of Permanent-magnet Synchronous Machines, IEEE Transactions on Industrial Electronics, 57(7), 2435–2443.

42. Bolognani, S., Peretti, L., Zigliotto, M., 2008. Parameter Sensitivity Analysis of an Improved Open-Loop Speed Estimate for Induction Motor Drives. IEEE Transactions on Power Electronics, 23(4), 2127–2135.

43. Ozturk, S.B., Akin, B., Toliyat, H.A., Ashrafzadeh, F., 2006. Low-cost Direct Torque Control of Permanent Magnet Synchronous Motor Using Hall-effect Sensors, 7–14.

44. Lu, Z., Sheng, H., Hess, H.L., Buck, K.M., 2005. The Modeling and Simulation of a Permanent Magnet Synchronous Motor with Direct Torque Control Based on Matlab/simulink, IEEE International Conference on Electric Machines and Drives, 7.

45. Seok, J.K., Lee, J.K., Lee, D.C., 2006. Sensorless Speed Control of Nonsalient Permanent-magnet Synchronous Motor Using Rotor-position-tracking PI Controller, IEEE Transactions on Industrial Electronics, 53(2), 399–405.

46. Stumberger, B., Stumberger, G., Dolinar, D., Hamler, A., Trlep, M., 2003. Evaluation of Saturation and Cross-magnetization Effects in Interior Permanent-magnet Synchronous

Motor, IEEE Transactions on Industry Applications, 39(5), 1264–1271.

47. Rusu, C., Radulescu, M.M., Enikö, S., Melinda, R.K., Jakab, Z.L., 2014. Embedded Motor Drive Prototype Platform for Testing Control Algorithms, International Conference on Applied and Theoretical Electricity (ICATE), 1–6.

48. Marcetic, D.P., Vukosavic, S.N., 2007. Speed-sensorless AC Drives with the Rotor Time Constant Parameter Update, IEEE Transactions on Industrial Electronics, 54(5), 2618–2625.

49. Mouna, B.H., Lassaad, S., 2006. Speed Sensorless Indirect Stator Field Oriented Control of Induction Motor Based on Luenberger Observer, IEEE International Symposium on Industrial Electronics, vol. 3, 2473–2478.

50. Shi, Y., Sun, K., Huang, L., Li, Y., 2012. Online Identification of Permanent Magnet Flux Based on Extended Kalman Filter for IPMSM Drive with Position Sensorless Control, IEEE Transactions on Industrial Electronics, 59(11), 4169–4178.